Supporting Information for "Graphene Plasmonics: A Platform for Strong Light-Matter Interaction"

Frank H. L. Koppens,[1,*] Darrick E. Chang,[2] and F. Javier García de Abajo[3,4,†]

[1] *ICFO-Institut de Ciéncies Fotóniques, Mediterranean Technology Park, 08860 Castelldefels (Barcelona), Spain*
[2] *Institute for Quantum Information, California Institute of Technology, Pasadena, CA 91125, USA*
[3] *Instituto de Óptica - CSIC, Serrano 121, 28006 Madrid, Spain*
[4] *Optoelectronics Research Centre, University of Southampton, Southampton SO17 1BJ, UK*

(Dated: April 11, 2011)

Contents

I. GRAPHENE CONDUCTIVITY IN THE RANDOM-PHASE APPROXIMATION (RPA)

The nonlocal conductivity is related to the susceptibility through

$$\sigma(k_\parallel,\omega) = -i\omega\chi_\tau(k_\parallel,\omega).$$

We introduce a finite relaxation time τ using the prescription given by Mermin [1, 2], which preserves the number of charge carriers:

$$\chi_\tau(k_\parallel,\omega) = \frac{(1+i/\omega\tau)\chi(k_\parallel,\omega+i/\tau)}{1+(i/\omega\tau)\chi(k_\parallel,\omega+i/\tau)/\chi(k_\parallel,0)},$$

where

$$\chi(k_\parallel,\omega) = \frac{e^2}{2\pi^2\hbar k_\parallel^2}\int d^2\mathbf{k}'_\parallel \sum_{s,s'=\pm}\left[1+ss'\frac{\mathbf{k}'_\parallel\cdot(\mathbf{k}_\parallel+\mathbf{k}'_\parallel)}{k'_\parallel|\mathbf{k}_\parallel+\mathbf{k}'_\parallel|}\right]\frac{\theta_F(s'v_F|\mathbf{k}_\parallel+\mathbf{k}'_\parallel|)-\theta_F(sv_Fk'_\parallel)}{\omega+v_F\left(sk'_\parallel-s'|\mathbf{k}_\parallel+\mathbf{k}'_\parallel|\right)+i0^+}$$

*Electronic address: frank.koppens@icfo.es
†Electronic address: J.G.deAbajo@csic.es

is the linear RPA response function [3, 4] and $\theta_F(E)$ is the Fermi-Dirac distribution.

The RPA response admits an analytical expression at zero temperature [3] (i.e., for $\theta_F(E) = \theta(E_F - E)$):

$$\chi(k_\parallel,\omega) = \frac{e^2}{4\pi\hbar}\left[\frac{8k_F}{v_F k_\parallel^2} + \frac{G(-\Delta_-)\,\theta\left[-\mathrm{Re}\{\Delta_-\}-1\right] + \left[G(\Delta_-)+i\pi\right]\,\theta\left[\mathrm{Re}\{\Delta_-\}+1\right] - G(\Delta_+)}{\sqrt{\omega^2 - v_F^2 k_\parallel^2}}\right],$$

where

$$G(z) = z\sqrt{z^2-1} - \log\left(z+\sqrt{z^2-1}\right)$$

and $\Delta_\pm = (\omega/v_F \pm 2k_F)/k_\parallel$. Here, the square roots are chosen to yield positive real parts, while the imaginary part of the logarithm is taken in the $(-\pi,\pi]$ range. Additionally, we have

$$\chi(k_\parallel,0) = \frac{e^2}{2\pi\hbar v_F k_\parallel}\left\{\frac{4k_F}{k_\parallel} - \theta(1-x)\left[x\sqrt{1-x^2} - \cos^{-1}x\right]\right\},$$

where $x = 2k_F/k_\parallel$. We use these formulas to compute the nonlocal RPA in this document.

To a good approximation (see below) the conductivity can be evaluated within the local RPA (i.e., the $k_\parallel \to 0$ limit), which leads to an analytical solution including the dependence on T [5]:

$$\begin{aligned}\sigma(\omega) =& \frac{2e^2T}{\pi\hbar}\frac{i}{\omega+i\tau^{-1}}\log\left[2\cosh(E_F/2k_BT)\right] \\ &+ \frac{e^2}{4\hbar}\left[H(\omega/2) + \frac{4i\omega}{\pi}\int_0^\infty d\varepsilon\,\frac{H(\varepsilon)-H(\omega/2)}{\omega^2-4\varepsilon^2}\right],\end{aligned} \tag{1}$$

where

$$H(\varepsilon) = \frac{\sinh(\hbar\varepsilon/k_BT)}{\cosh(E_F/k_BT)+\cosh(\hbar\varepsilon/k_BT)}.$$

The first term in Eq. (1) corresponds to intra-band transitions, in which the relaxation time has been introduced to make it converge to the Drude model at $T = 0$. We show below that nonlocal effects produce qualitatively similar results as a finite relaxation time τ and temperature T. Because the actual value of τ depends on the quality of the synthetized graphene, it can actually be regarded as an effective parameter. Actually, the decay rate of an emitter in the vicinity of homogeneous graphene is rather insensitive to the inclusion of nonlocal effects and the actual value of τ and T within the wide spectral region for which the plasmons are well defined (see below). Therefore, we use Eq. (1) for the conductivity in all calculations presented here and in the main paper (unless it is stated otherwise) because it gives a reasonable description and it is local, so that we assume that it can be also used for patterned graphene.

When $T = 0$, Eq. (1) reduces to

$$\sigma(\omega) = \frac{e^2E_F}{\pi\hbar^2}\frac{i}{\omega+i\tau^{-1}} + \frac{e^2}{4\hbar}\left[\theta(\hbar\omega-2E_F) + \frac{i}{\pi}\log\left|\frac{\hbar\omega-2E_F}{\hbar\omega+2E_F}\right|\right], \tag{2}$$

which shows a sudden increase in losses (step function affecting the real part of σ) at the onset of vertical intra-band transitions, $\hbar\omega = 2E_F$. Full inclusion of finite temperature and damping leads to a smoother onset, but Eq. (2) contains the main features of the graphene conductivity.

II. FRESNEL COEFFICIENTS AND PLASMON DISPERSION IN HOMOGENEOUS GRAPHENE

The response of homogeneous graphene is expressed in terms of its Fresnel reflection coefficients [6], which can be obtained by applying the customary boundary conditions ($\Delta\mathbf{E}_\parallel = \Delta\mathbf{H}_\perp = 0$, $\Delta(\epsilon\mathbf{E}_\perp) = 4\pi\sigma\nabla\cdot\mathbf{E}_\parallel/i\omega$, and $\hat{\mathbf{n}}\times\Delta\mathbf{E}_\perp = (4\pi\sigma/c)\mathbf{E}_\parallel$) for the fields of incoming p- and s-polarized plane waves as

$$\begin{aligned} r_p &= \frac{\epsilon k_\perp - k'_\perp + 4\pi\sigma k_\perp k'_\perp/\omega}{\epsilon k_\perp + k'_\perp + 4\pi\sigma k_\perp k'_\perp/\omega}, \\ r_s &= \frac{k_\perp - k'_\perp + 4\pi\sigma k_0/c}{k_\perp + k'_\perp + 4\pi\sigma k_0/c}, \end{aligned} \tag{3}$$

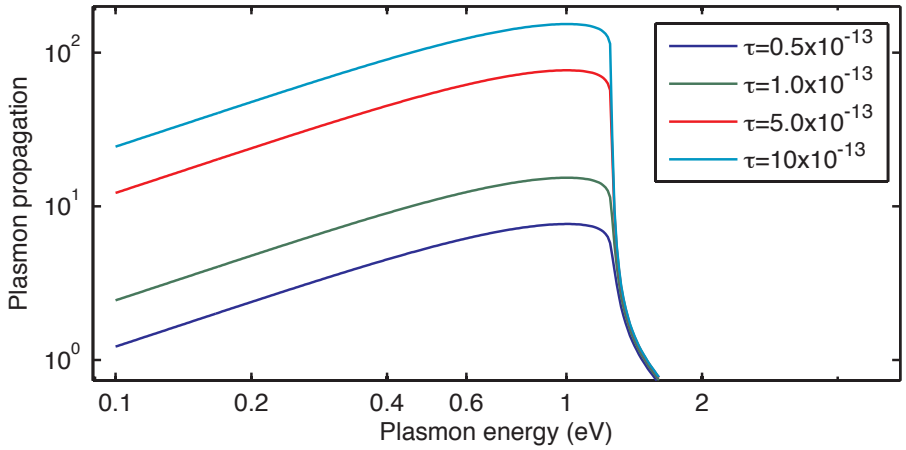

FIG. 1: Spectral dependence of the in-plane plasmon propagation distance (in units of the plasmon wavelength) obtained from the RPA for various relaxation times in homogeneous graphene supported on an $\epsilon = 2$ material and doped to $E_F = 1\,\mathrm{eV}$.

where ϵ is the permittivity of the substrate on which the graphene is deposited, $k_0 = \omega/c$ is the free-space light wave vector, $k_\perp = \sqrt{k_0^2 - k_\parallel^2}$ and $k'_\perp = \sqrt{\epsilon k_0^2 - k_\parallel^2}$ are the perpendicular wave vectors outside and inside the substrate, respectively, and $k_\parallel$ is the parallel wave vector.

The dispersion relation of p-polarized surface plasmons (SPs) is determined by the pole of r_p, which yields the equation

$$\epsilon/\sqrt{\epsilon k_0^2 - k_{\mathrm{sp}}^2} + 1/\sqrt{k_0^2 - k_{\mathrm{sp}}^2} = -4\pi\sigma/\omega$$

for the plasmon wave vector k_{sp}. Here, we can use the electrostatic limit of this expression,

$$k_{\mathrm{sp}} \approx i(\epsilon + 1)\omega/4\pi\sigma,$$

under the common condition $k_0 \ll |k_{\mathrm{sp}}|$ (actually, this condition is fulfilled for $\hbar\omega \gg \alpha E_F$, where $\alpha \approx 1/137$ is the fine-structure constant).

We plot the plasmon dispersion relation in Fig. 1 of the main paper, and we supplement it here by showing the $1/e$-amplitude-decay propagation length computed from $1/\mathrm{Im}\{k_{\mathrm{sp}}\}$ as a function of plasmon energy for various values of τ. For the relaxation times considered in this work, the susceptibility has an almost linear dependence on the damping rate $1/\tau$ that translates into a linear variation of the plasmon propagation length with this parameter, as shown in Fig. 1 for $E_F = 1\,\mathrm{eV}$.

III. DECAY RATE AND ITS DEPENDENCE ON CONDUCTIVITY MODEL, TEMPERATURE, AND RELAXATION TIME

The decay rate Γ can be related to the electric field induced by a dipole $\mathbf{d}$ on itself $\mathbf{E}^{\mathrm{ind}}$ as [6]

$$\Gamma = \Gamma_0 + \frac{2}{\hbar}\mathrm{Im}\{\mathbf{d}^* \cdot \mathbf{E}^{\mathrm{ind}}\}, \tag{4}$$

where $\Gamma_0 = 4k_0^3|\mathbf{d}|^2/3\hbar$ is the free-space decay rate. When the emitter is above a substrate covered with a homogeneous graphene layer, the induced or reflected field can be in turn related to the Fresnel coefficients of graphene to yield [6]

$$\Gamma = \Gamma_0 + \frac{1}{\hbar}\int_0^\infty k_\parallel\, dk_\parallel\, \mathrm{Re}\left\{\left[|\mathbf{d}_\parallel|^2(k_0^2 r_s - k_\perp^2 r_p) + 2|\mathbf{d}_\perp|^2 k_\parallel^2 r_p\right]\frac{e^{2ik_\perp z}}{k_\perp}\right\}, \tag{5}$$

where z is the emitter-graphene separation, $\mathbf{d}_\parallel$ and $\mathbf{d}_\perp$ are the components of the transition dipole parallel and perpendicular to the carbon plane, and the integral is extended over parallel wave vectors $k_\parallel$. In this work, we use

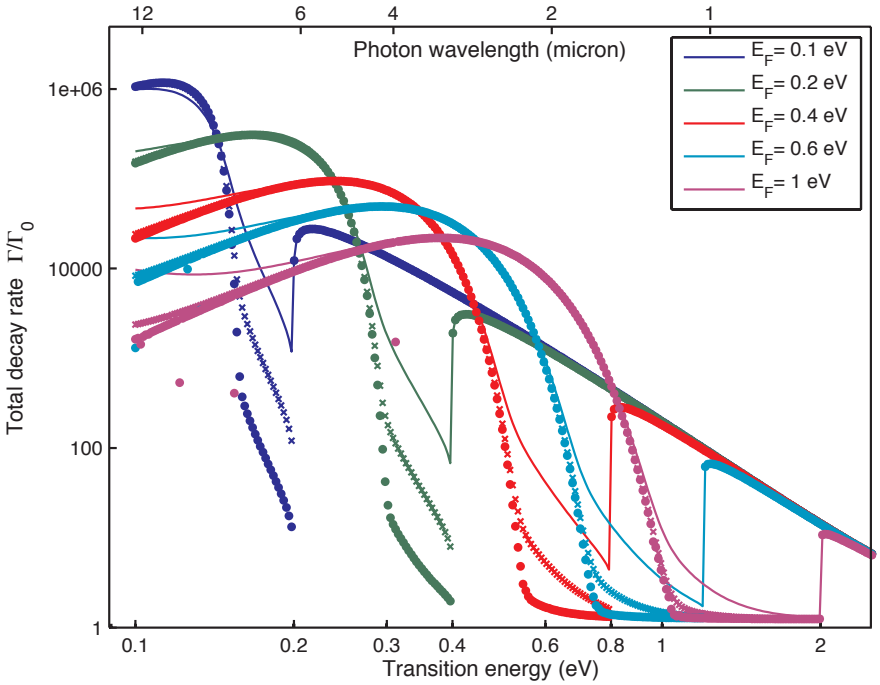

FIG. 2: Decay rate calculated from the RPA at $T = 0$ for $\tau = 50\,\mathrm{fs}$ (solid curves), $\tau = 500\,\mathrm{fs}$ (crosses), and $\tau = 5,000\,\mathrm{fs}$ (dots). The emitter is placed 10 nm away from a homogeneous graphene sheet deposited on the surface of an $\epsilon = 2$ material. The rate Γ is normalized to the free-space rate Γ_0.

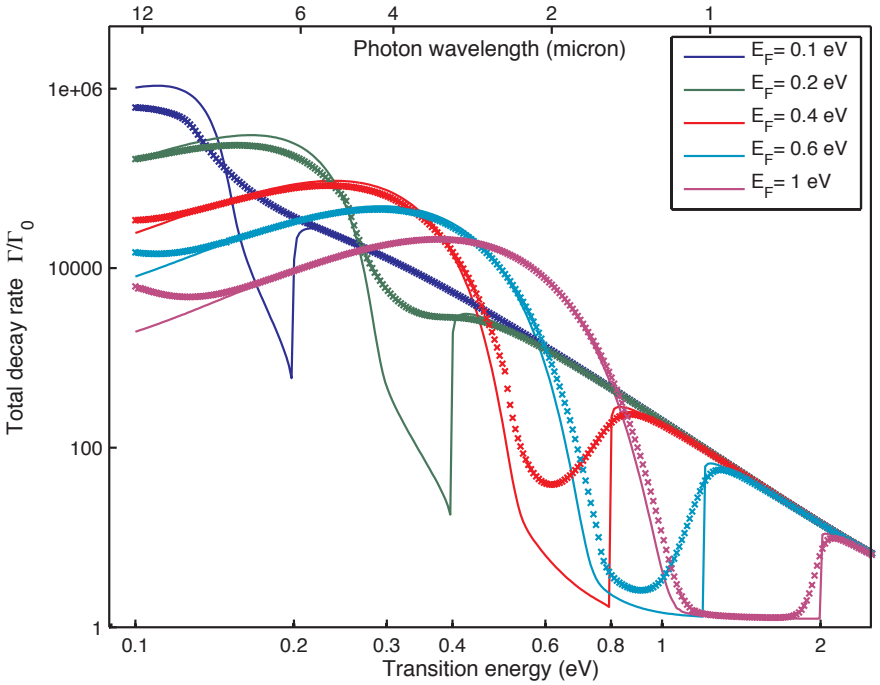

FIG. 3: Decay rate obtained from the RPA (symbols) and the local RPA (curves) under the same conditions as in Fig. 2 with $T = 0$, $\tau = \mu E_F/ev_F^2$, and a mobility $\mu = 10,000\,\mathrm{cm}^2/\mathrm{Vs}$ (e.g., $\tau \approx 10^{-13}\,\mathrm{s}$ for $E_F = 0.1\,\mathrm{eV}$).

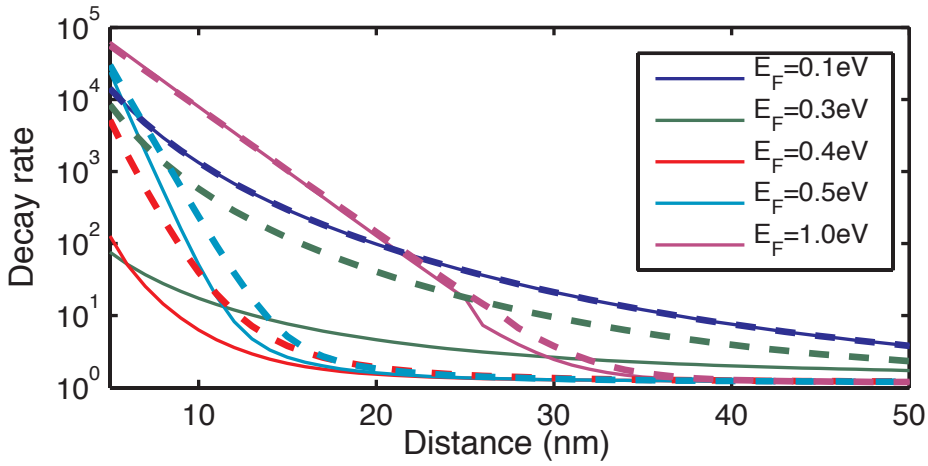

FIG. 4: Distance dependence of the decay rate under the conditions of Fig. 3 for a photon energy of 0.5 eV. Solid curves: local RPA. Dashed curves: RPA.

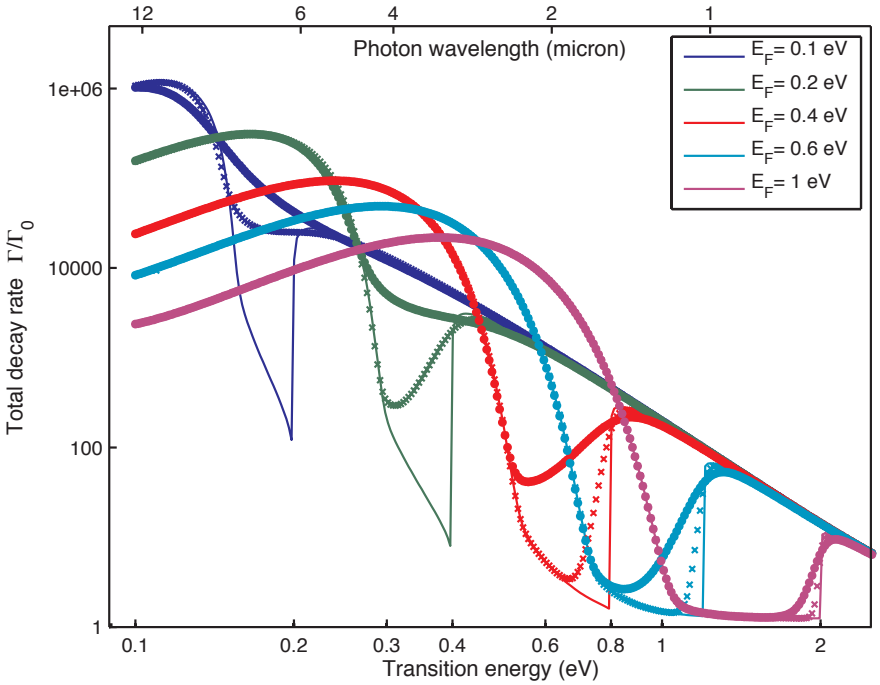

FIG. 5: Decay rate calculated from the local RPA at $T = 0$ (solid curves), $T = 100$ (crosses), and $T = 300$ (dots) for $\tau = 500$ fs under the same conditions as in Fig. 2.

Eq. (5) to compute the decay rate in homogeneous graphene, and Eq. (4) for nanoribbons and nanodisks, with $\mathbf{E}^{\rm ind}$ calculated as explained in Sec. IV and V.

The decay rate Γ is a $k_{\parallel}$-integrated quantity, and therefore, we expect a mild dependence on the relaxation time τ, except in the neighborhood of the onset of vertical inter-band transitions, where Γ takes small values that are incremented by the smearing of the electron-hole pair (e-h) continuum due to relaxation. This is the conclusion that can be extracted from Fig. 2, in which we plot the spectral dependence of Γ for various values of the Fermi energy and

we consider a wide range of relaxation parameters. The rate is nearly independent of τ over the region of existence of surface plasmons and also above the noted onset, where it convergences to the undoped graphene level.

A similar conclusion can be drawn when comparing the RPA with the local RPA (Fig. 3). They produce nearly the same results, except in the spectral region extending from the plasmon cutoff to the vertical inter-band transition threshold. Clearly, the agreement in the plasmon region improves for higher E_F, presumably as a result of the momentum cutoff for finite separation between the emitter and the graphene, which effectively reduces the effect of non-vertical e-h transitions. The two models also differ in the low-energy region. The agreement in the plasmonic region is also observed in the distance dependence of Γ (Fig. 4), although severe discrepancies are observed for E_F slightly below the photon energy.

We explore the variation with temperature in Fig. 5. The effect of a finite temperature is similar to that of finite relaxation, essentially consisting in smearing the dip in the decay rate below the $2E_F$ onset.

IV. FOURIER EXPANSION METHOD FOR NANORIBBONS

We consider a nanoribbon contained in the $z = 0$ plane and having translational invariance along y. Furthermore, we assume the external field to be independent of y. This is the case for illumination with a plane wave normal to the graphene and polarized along x (actually, this is the geometry for which we calculate the cross section in this work), and also for emission from a line dipole polarized along either x or z and consisting of a continuous distribution of identical point dipoles distributed along a line parallel to y (we obtain decay rates for this configuration).

Under these conditions, the component of the electric field parallel to the graphene is along x, and thus, the induced current $\eta(x)$ is also along x. The field produced by each surface element $dxdy$ is the same as that of a dipole $(i\eta/\omega)\,dxdy$. Summing all of these dipole contributions, and including the effect of a substrate through its Fresnel coefficients [6], we find the self-consistent relation

$$\eta(x)/\sigma = E_x^{\rm ext}(x) - \frac{1}{\omega}\int dq\; k_\perp(1-r_p)\int dx' e^{iq(x'-x)}\eta(x'), \tag{6}$$

where the x integral is extended over the graphene width, $k_\perp = \sqrt{k_0^2 - q^2}$, k_0 is the free-space light wave vector, and r_p is the Fresnel coefficient of the substrate for p polarization. More precisely, $r_p = (\epsilon k_\perp - k'_\perp)/(\epsilon k_\perp + k'_\perp)$, where $k'_\perp = \sqrt{\epsilon k_0^2 - q^2}$. Here, $E_x^{\rm ext}$ is the external electric field along x, which already includes the reflection by the homogeneous dielectric substrate of permittivity ϵ.

We solve Eq. (6) by considering a supercell with the graphene occupying the $z = 0$ and $0 < x < b$ region, and by periodically repeating this unit cell with period a along x. Then, we expand the conductivity, the external field, and the surface current in Fourier series. For example, the conductivity becomes

$$\sigma(x) = \sum_n \sigma_n e^{ig_n x}$$

(it is zero outside the graphene and given by Eq. (1) in the graphene), where $g_n = 2\pi n/a$, and the coefficients σ_n are easily obtained from the expansion of the step function representing the ribbon. This allows us to project Eq. (6) into Fourier components as

$$\eta_n = \frac{1}{a}\int_0^b dx\,\sigma(x)\,E_x^{\rm ext}(x)\,e^{-ig_n x} - \frac{2\pi}{\omega}\sum_{n'} k_\perp^{n'}(1-r_p^{n'})\sigma_{n-n'}\eta_{n'}, \tag{7}$$

where $k_\perp^{n'}$ and $r_p^{n'}$ are the same as $k_\perp$ and r_p for $q = g_{n'}$. Finally, we solve Eq. (7) by using standard linear algebra with a finite number of waves M.

The scattered near-field is given in terms of the η_n coefficients as

$$\mathbf{E}^{\rm scat} = -\frac{2\pi}{\omega}\sum_n \eta_n\, e^{ig_n x} \times \begin{cases} e^{ik_\perp^n z}(1-r_p^n)\;(k_\perp^n, 0, -g_n), & z > 0, \\ e^{-ik'^n_\perp z}(1+r_p^n)\;(k'^n_\perp, 0, g_n)/\epsilon, & z < 0, \end{cases}$$

where the substrate is taken to occupy the $z < 0$ region.

We obtain convergence for isolated ribbons by taking a equal to 2-4 times b. Then, we derive the single-ribbon far-field from the induced current of the ribbon in the first unit cell:

$$\mathbf{E}^{\rm scat} = \frac{e^{ik'R}}{\sqrt{k'R}}\,f\,\hat{\varepsilon}_p,$$

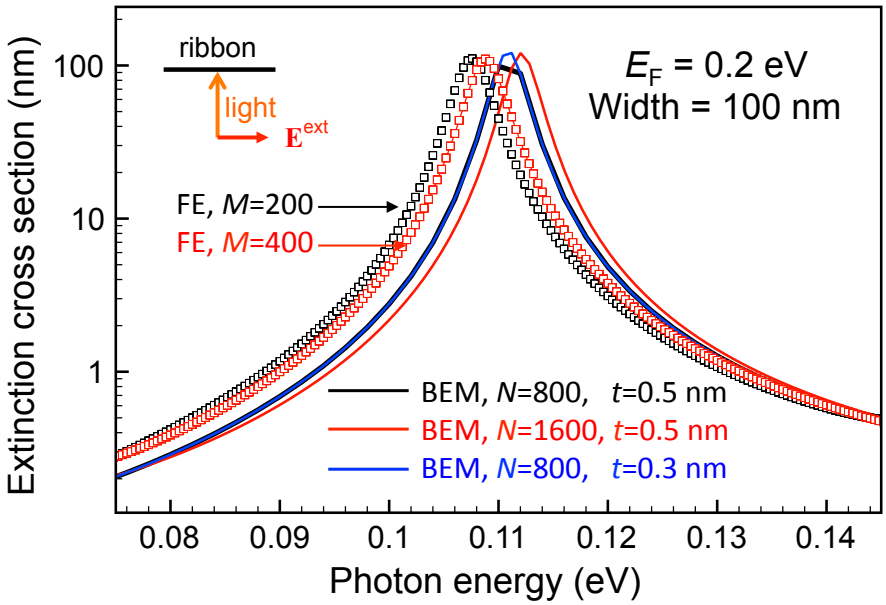

FIG. 6: Convergence of the Fourier expansion (FE) and the boundary element method (BEM) for a graphene nanoribbon of width 100 nm and $E_F = 0.2$ eV. We represent the extinction cross section calculated with various values of the convergence parameters for normally-incident light. The number of Fourier components M and boundary parametrization points N are given in the text labels.

where $\hat{\varepsilon}_p$ is the unit vector for scattered p-polarized light,

$$f = \frac{\sqrt{2\pi}k_0}{c} e^{i\pi/4}(1 \pm r_p)\ \cos\theta \sum_n \eta_n I_n \tag{8}$$

is the field amplitude, θ is the angle relative to the outwards surface normal, $k' = k_0$ ($k' = k_0\sqrt{\epsilon}$) above (inside) the substrate, the upper (lower) sign in (8) applies outside (inside) the substrate, and

$$I_n = \frac{e^{i(g_n - q)b} - 1}{g_n - q}.$$

Here, the reflection coefficient r_p and the parallel wave vector $q = k_0 \sin\theta$ are determined by the outgoing angle θ.

Applying the optical theorem to the transmitted and reflected light upon plane wave illumination and using the above expressions for the far field, we find the extinction cross section

$$\sigma^{\text{ext}} = \frac{8\pi}{\omega} \frac{k_\perp k'_\perp}{\epsilon k_\perp + k'_\perp} \text{Im}\left\{ -\sum_n \eta_n I_n \right\}.$$

Finally, the decay rate per unit length along y for a line dipole of per-unit-length strength $\mathbf{d}$ ($\perp y$) situated above the substrate is calculated from

$$\Gamma = \frac{\pi k_0^2 d^2}{\hbar} + \frac{2}{\hbar}\text{Im}\{\mathbf{E}^{\text{ind}} \cdot \mathbf{d}\},$$

where the induced field is evaluated at the position of the dipole.

V. CONVERGENCE OF FOURIER EXPANSION AND BOUNDARY ELEMENT METHOD

The Fourier expansion method converges when the number of Fourier coefficients is increased, as we show in Fig. 6 (symbols). This method produces results in excellent agreement with an alternative approach fully relying on numerical simulations, consisting in modeling the graphene as a thin film of dielectric function $1 + 4\pi i\sigma/\omega t$ and

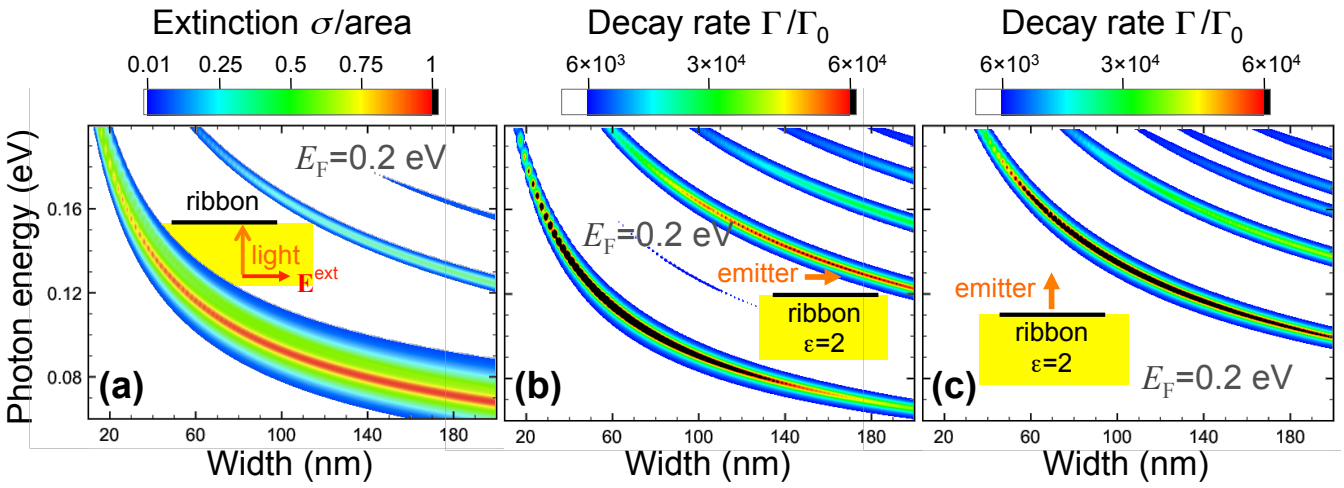

FIG. 7: **(a)** Extinction cross section of doped graphene ribbons deposited on an $\epsilon = 2$ material as a function of ribbon width and photon energy for a Fermi energy $E_F = 0.2\,\mathrm{eV}$. The light is incident as shown in the inset. The cross section is normalized to the carbon sheet area. **(b,c)** Decay rate normalized to free space under the same conditions as in (a) for a line emitter situated 10 nm above the center of the ribbon and polarized either parallel (b) or perpendicular (c) to it.

thickness t, with the edges rounded by hemi-circular profiles, for which we find converged electromagnetic results using the boundary element method (BEM) [7], as shown in Fig. 6 (solid curves).

The agreement between the semi-analytical Fourier expansion and the BEM confirms the validity of the latter to describe graphene as a thin effective layer of dielectric. Actually, we use this method to simulate graphene disks, because an analytical expansion for them becomes too involved and does not add much insight into the problem.

VI. SUPPORTED VS SELF-STANDING NANORIBBONS

We show in Fig. 7 calculations similar to those of Fig. 3 of the main paper, but for graphene ribbons supported on the surface of an $\epsilon = 2$ material rather than self-standing. The results are qualitatively the same for supported and for self-standing graphene. The extinction cross section and the decay rates have similar magnitude in both cases. The only difference that is worth noticing is the redshift in the plasmon energy in the supported graphene, which is consistent with the scaling of $\omega \propto 1/\sqrt{\epsilon + 1}$ predicted by the Drude model.

VII. DISTANCE DEPENDENCE OF THE DECAY RATE NEAR A NANODISK

In the main paper, we have discussed the decay rate for an emitter situated at a fixed point along the axis of self-standing circular graphene disks. Here we consider the variation of the peak decay rate as a function of position of the emitter. Figure 8a shows the variation of the rate with distance to the graphene along the axis of the disk. The rate decays with distance z roughly as $\exp(-4\pi z/\lambda_{\mathrm{sp}})$ (i.e., it follows the same exponential attenuation as in homogeneous graphene), where the plasmon wavelength λ_{sp} is 290 nm for the $m = 1$ mode and 94 nm for the $m = 0$ mode. The variation along parallel displacements (Fig. 8b) is less trivial, but it qualitatively follows the near-field intensities shown in Fig. 4c,d of the main paper.

VIII. PLASMONS IN GRAPHENE NANODISKS: SIZE, DOPING, AND RELAXATION DEPENDENCE

Figure 9 summarizes the E_F and disk-size dependence of SPs in graphene nanodisks. The evolution of the plasmon energy is inherited from the $\omega_p \propto \sqrt{E_F/\lambda_{\mathrm{sp}}}$ scaling in homogeneous graphene, so that it increases with $\sqrt{E_F}$ (Fig. 9a) and decreases with the inverse of the square root of the radius (Fig. 9b).

The peak decay rate has a weak dependence on both E_F and disk size (Fig. 9c,d), essentially reflecting the increase in SP lifetime when its energy is positioned close to E_F. Maximum rates $\sim 10^6\,\Gamma_0$ are consistently obtained near

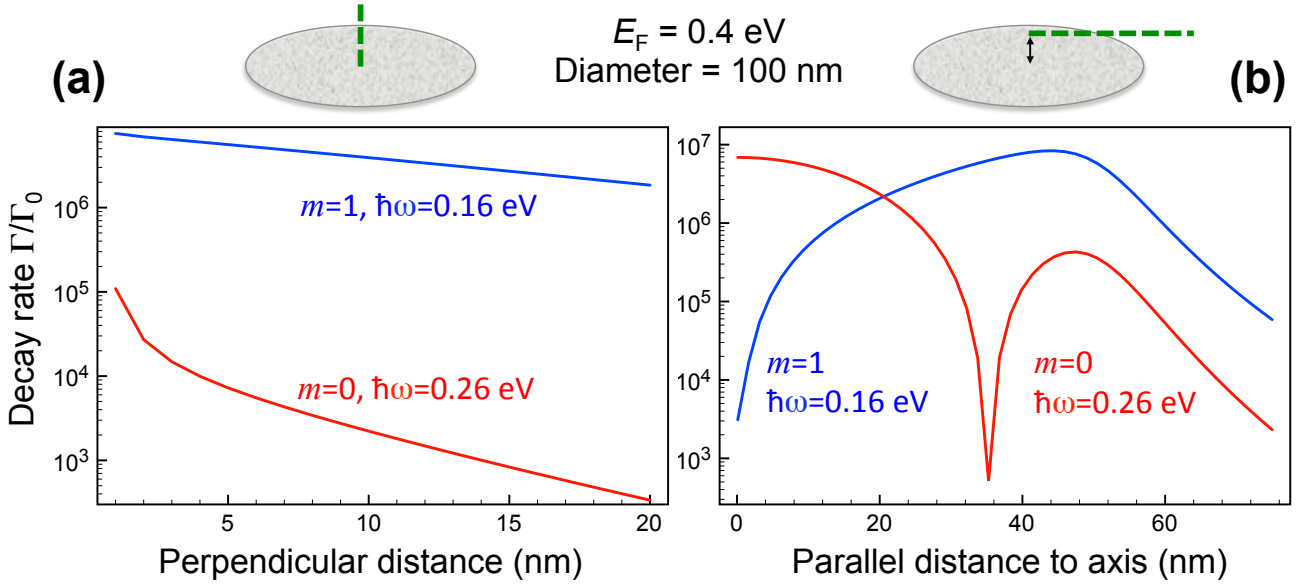

FIG. 8: Position dependence of the decay rate Γ near a self-standing graphene disk of diameter 100 nm and $E_F = 0.4$ eV. The rate is given as a function of position along the dashed-line excursions shown in the upper insets. Plot (b) is obtained for a distance of 10 nm from the graphene plane. The rate is calculated at the peak position of the lowest-order $m = 1$ and $m = 0$ resonances, respectively (see Fig. 4 of the main paper).

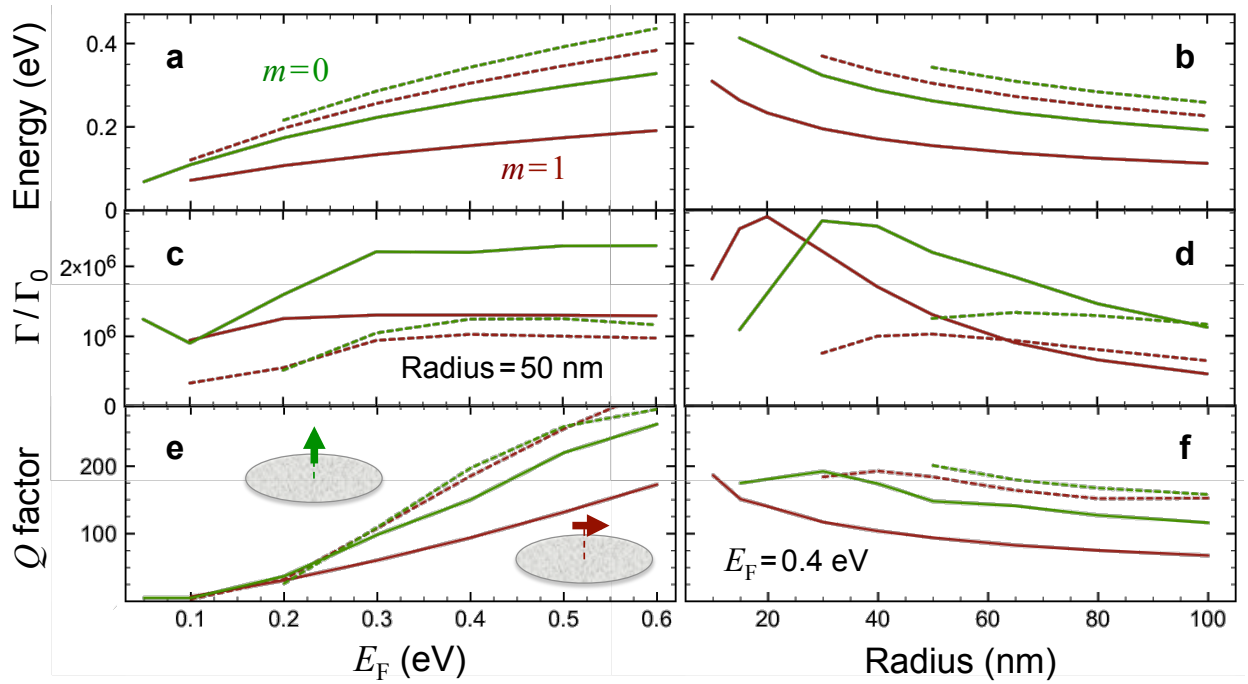

FIG. 9: **Plasmons in graphene nanodisks: Size and doping dependence.** **(a,b)** Fermi-energy and disk-radius dependence of the SP energy in doped graphene disks for the first- (solid curves) and second-order (dashed curves) modes with either $m = 0$ (green curves) or $m = 1$ (red curves) azimuthal symmetries. The two lowest-order modes are shown for each symmetry. **(c,d)** Decay rate Γ of an emitter located 10 nm above the center of the disk, normalized to the rate in free space Γ_0, and calculated at the energies of the SPs in (a,b). The emitter is polarized parallel (perpendicular) to the disk in the red (green) curves. **(e,f)** Quality factor of the resonances considered in (a,b).

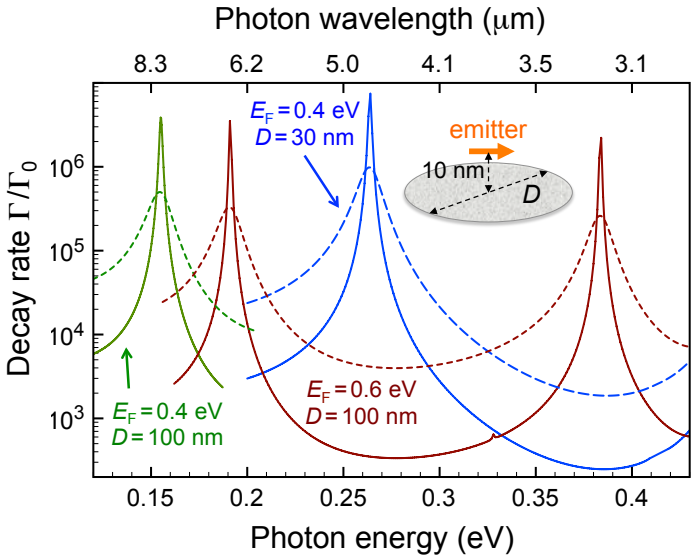

FIG. 10: **Plasmons in graphene nanodisks: Relaxation dependence.** Decay rate of an emitter situated 10 nm above the center of a doped graphene disk for two different disk diameters D and two values of the Fermi energy E_F, as shown by text labels. The emitter is polarized parallel to the disk. Dashed curves are calculated with $\tau \sim 0.5 \times 10^{-13}$ s. Solid curves are obtained with $\tau = 4 \times 10^{-13}$ s for $E_F = 0.4$ eV and $\tau = 6 \times 10^{-13}$ s for $E_F = 0.6$ eV.

these disks at the distance $z = 10$ nm chosen in the calculations.

The quality factor of the SP resonances Q (Fig. 9e,f, extracted from the peak frequency divided by the FWHM) shows a strong increase with E_F, in agreement with the longer propagation distance observed in homogeneous graphene at higher doping. Our reported values of $Q > 100$ are consistent with the moderate relaxation time employed in the calculations, $\tau \approx 10^{-13}$ s (i.e., $Q \sim \omega_p \tau$). Actually, the values of Q reported in Fig. 9e,f are qualitatively well predicted by this formula using the energies of Fig. 9a,b as input. At the same time, much higher values of the mobility μ have been reported[8], which should lead to larger Q's and peak rates in direct proportion to μ, at least below the optical phonon frequency.

The role of plasmons in the relaxation of graphene is not yet well understood, although careful analysis [2] reveals that their effect can be incorporated through an effective $\tau \sim 0.5 \times 10^{-13}$ s. We show in Fig. 10 results for the decay rate near nanodisks obtained with this effective value of τ (dashed curves), compared to calculations obtained with $\tau = \mu E_F / e v_F^2$ and a mobility $\mu = 10,000\,\mathrm{cm}^2/\mathrm{Vs}$ (solid curves, taken from Fig. 4 of the main paper). The shorter relaxation time due to phonons produces a decrease in both the peak rate and Q by a factor of ∼5-9 in the spectra shown here, which increases linearly with E_F and decreases smoothly with ω.

IX. FIELD LINES IN NEAR-FIELD PLOTS

The near-electric-fields shown in the main paper for ribbons and disks are obtained close to a non-degenerate resonance at $\omega = \omega_0$, so that they take the form $\mathbf{E}^{\mathrm{ext}} + \mathbf{F}/(\omega_0 - \omega - i\gamma/2)$, where γ is the plasmon relaxation rate. Since the ribbon width is much smaller than the light wavelength, the near field must be almost electrostatic, and therefore, $\mathbf{E}$ and $\mathbf{F}$ are approximately real vectors. Interestingly, the on-resonance induced field $i2\mathbf{F}/\gamma$ is almost imaginary, in good agreement with our numerical simulations. Using a real transition dipole, the induced fields plotted in the main paper are more than 99% imaginary, and this actually allows us to extract the field lines that are shown there (i.e., field lines corresponding to a nearly real, electrostatic electric field).

X. POLARIZABILITY OF THE COMBINED SP-EMITTER SYSTEM IN THE JAYNES-CUMMINGS MODEL

The interaction with the external field $E(t)$ can be written

$$H_{\mathrm{ext}} = -(P_p + P_0)\, E(t),$$

which involves the plasmon and emitter dipole operators $P_p = d_p a + d_p^* a^+$ and $P_0 = d_0\sigma + d_0^*\sigma^+$, where d_p and d_0 are their respective transition dipoles.

We derive the polarizability α from the first-order-perturbation-theory steady-state solution of the model Hamiltonian for a faint external field of the form $E(t) = 2\mathrm{Re}\{E_0 e^{-i\omega t}\}$. The polarizability is defined through the relation $p(t) = 2\mathrm{Re}\{\alpha(\omega)E_0 e^{-i\omega t}\}$, obtained from the expected value of the combined induced dipole, $p = \langle P_p + P_0\rangle$. After some algebra, we find

$$\alpha(\omega) = \alpha_0(\omega) + \alpha_0^*(-\omega),$$

where

$$\alpha_0(\omega) = \frac{(\omega_0 - \omega - i\Gamma_0/2)|d_p|^2 + (\omega_p - \omega - i\kappa/2)|d_0|^2 - 2g\mathrm{Im}\{d_p d_0^*\}}{(\omega_0 - \omega - i\Gamma_0/2)(\omega_p - \omega - i\kappa/2) - g^2}.$$

In the calculations presented in Fig. 5c of the main paper we assume d_0 to be negligible compared to d_p. Furthermore, the model parameters ω_p, Γ, and Q are extracted from the second $m = 1$ mode of Fig. 9a,c,e (red dashed curves) following the procedure described in the main paper.

[1] Mermin, N. D. Lindhard dielectric function in the relaxation-time approximation. *Phys. Rev. B* **1**, 2362–2363 (1970).

[2] Jablan, M., Buljan, H. & Soljačić, M. Plasmonics in graphene at infrared frequencies. *Phys. Rev. B* **80**, 245435 (2009).

[3] Wunsch, B., Stauber, T., Sols, F. & Guinea, F. Dynamical polarization of graphene at finite doping. *New J. Phys.* **8**, 318 (2006).

[4] Hwang, E. H. & Das Sarma, S. Dielectric function, screening, and plasmons in two-dimensional graphene. *Phys. Rev. B* **75**, 205418 (2007).

[5] Falkovsky, L. A. & Varlamov, A. A. Space-time dispersion of graphene conductivity. *Eur. Phys. J. B* **56**, 281 (2007).

[6] Novotny, L. & Hecht, B. *Principles of Nano-Optics* (Cambridge University Press, New York, 2006).

[7] García de Abajo, F. J. & Howie, A. Retarded field calculation of electron energy loss in inhomogeneous dielectrics. *Phys. Rev. B* **65**, 115418 (2002).

[8] Bolotin, K. I. *et al.* Ultrahigh electron mobility in suspended graphene. *Sol. State Commun.* **146**, 351–355 (2008).